Estimation of the vortex length scale and intensity from two-dimensional samples

By D. L. Reuss[1] AND W. P. Cheng,[2]

A method is proposed for estimating flow features that influence flame wrinkling in reciprocating internal combustion engines, where traditional statistical measures of turbulence are suspect. Candidate methods were tested in a computed channel flow where traditional turbulence measures are valid and performance can be rationally evaluated.

Two concepts are tested. First, spatial filtering is applied to the two-dimensional velocity distribution and found to reveal structures corresponding to the vorticity field. Decreasing the spatial-frequency cutoff of the filter locally changes the character and size of the flow structures that are revealed by the filter. Second, vortex length scale and intensity is estimated by computing the ensemble-average velocity distribution conditionally sampled on the vorticity peaks. The resulting conditionally sampled "average vortex" has a peak velocity less than half the rms velocity and a size approximately equal to the two-point-correlation integral-length scale.

1. Introduction

The existence of turbulence is central to the operation of reciprocating internal-combustion (RIC) engines. In particular, turbulence controls the burning rates (and thus the efficiency and engine speed range) in homogeneous charge engines by controlling flame wrinkling and in stratified charge engines by controlling mixing rates. However, considerable controversy exists concerning the definition and measurement of the turbulence properties in RIC engines. The purpose of this work is to explore new ways of estimating the turbulence properties that affect flame wrinkling in a way that will overcome the problems of defining turbulence.

1.1 Turbulent flow in RIC engines

The flow field in the engine cylinder is first formed during the intake stroke as the air enters the engine cylinder through the annular gap between the inlet volume and the cylinder head. The flow is driven by the piston moving from top to bottom dead center. This forms very large scale motions (on the order of the cylinder diameter) often referred to as the "mean" flow. A strong swirling flow (similar to a single tornado filling the cylinder) is an example of the simplest mean flow that can be formed. The flow is then compressed as the piston moves up. Measurements and computations both suggest that the turbulent kinetic energy generated by the valve jets has largely decayed by top dead center, TDC. The turbulent kinetic energy that

1 General Motors Research & Environmental Staff, Warren, MI

remains near TDC (when combustion begins) is generated mostly by the breakdown of the large-scale mean-flow structures. As the engine cycle continues, the flow is further distorted during combustion by the expansion of hot product gases and by the piston motion during the expansion stroke. Finally, the burnt gases are expelled through the exhaust valve by the piston motion during the exhaust stroke.

The problem in defining RIC engine turbulence is rooted in what will be referred to here as "traditional turbulence theory", in particular, the traditional Eulerian point of view where the turbulent velocity, $u(t)$, is measured at a fixed point as a function of time. The Reynolds decomposition is invoked,

$$u = \overline{u} + u', \tag{1}$$

where $\overline{u}$ is the steady (or at least slowly varying) mean and u' is the fluctuating component. For the Reynolds decomposition to be valid, it is implicit that the temporal (and spatial) variations in $\overline{u}$ occur over times (and distances) that are large compared to those associated with variations in u'. Further, the traditional flow is statistically stationary so that temporal averaging can be performed where local homogeneity exists and spatial averaging can be performed where directional homogeneity exists.

Extending these traditional concepts to RIC engines is difficult at best (Arcoumanis & Whitelaw 1987, le Coz 1992, Fansler & French 1988, Fransler 1993, Fraser & Bracco 1988, Glover 1986, Rask 1981 & 1984). The velocity distribution of the largest structures associated with the "mean flow" is not steady, and the structures' spatial scales change due to dissipation and volume changes forced by the piston. Thus, simple temporal averaging cannot be used. Instead, the Eulerian velocity is conditionally sampled at each crank-angle during the engine cycle (eg. at each 720 degrees of a four-stroke- cycle engine or 360 degrees in a two-stroke-cycle engine) and ensemble averaged over many cycles. The fluctuations about this mean that would traditionally be viewed as turbulence are not statistically stationary during the cycle, and there is no clear separation of the spatial and temporal scales of the ensemble mean velocity and turbulence. There is no local or directional homogeneity for temporal or spatial averaging.

Further complicating the interpretation of RIC engine turbulence is the fact that cyclic variability in the mean flow contributes to measured fluctuations about the ensemble-mean velocity. Consider the swirling flow example above, but with no small scale random fluctuations normally associated with turbulence (ie. a laminar tornado). Let the center of the swirl (the point of zero velocity) randomly precess about the geometric center of the engine cylinder. Here the cyclic variability would be the phase variation in the position of the swirl center from cycle to cycle. That is, a fixed velocity probe might be precisely at the swirl center at a specific crank angle during one cycle and thus measure zero velocity, yet be near but outside the swirl center at the same crank angle during the next cycle and thus measure some finite velocity. By ensemble averaging many cycles at the same position and crank angle, a fluctuating velocity component is measured about the ensemble mean velocity. Whereas cyclic variability of the swirling flow would be expected to convect the flame

to different positions on different cycles, it would not contribute to flame wrinkling to control the burning rate as turbulence does. Further, this fluctuating velocity does not correspond to the traditional concepts of fluctuations that contribute to the dissipation of turbulent kinetic energy. In reality, the flow actually does contain small-scale random turbulent structures and thus the measured velocity fluctuation in eqn. 1, u', is a sum of both the cyclic variability and the turbulence fluctuation. Consequently, estimates of the turbulence intensity, and thus kinetic energy, using u' will be overestimated, and turbulence length-scale estimates using two-point correlations will be incorrect.

In an attempt to separate the cyclic variability of the mean flow from the turbulence (Fansler & French 1988, Fraser & Bracco 1988), the instantaneous velocity has been separated as follows,

$$u = \langle u \rangle + u' \tag{2}$$

$$= \langle u \rangle + \tilde{u} + u'' \tag{3}$$

$$u = \langle U \rangle + u'' \tag{4}$$

where $\langle u \rangle$ is the ensemble mean, u' is the fluctuation about $\langle u \rangle$, $\tilde{u}$ is the cyclic fluctuation, u'' is the turbulence fluctuation, and $\langle U \rangle$ is the cycle resolved mean. In practice, $\tilde{u}$ and u'' are the low- and high-pass filtered components of u', respectively, where an engine-speed-dependent cutoff frequency between 100 and 500 Hz is typically assigned (Rask 1981 & 1984).

The content of the cyclic fluctuations and turbulence fluctuations is dependent on this cutoff frequency and is technically incorrect if, as expected, the energy spectra (temporal and spatial scales) of $\tilde{u}$ and u'' overlap.

In summary, the problem defining turbulence in RIC engines is that it has an unsteady mean with cycle-to-cycle variability, the temporal and spatial scales of the mean flow and turbulence fluctuations overlap, and in general the flow is inhomogeneous and anisotropic in all directions. Although velocity measurements have been used to illustrate the problem, the question of separating cyclic variability from turbulence is equally important in CFD modeling of in-cylinder combustion since single time- and length-scale models (usually $k - \epsilon$ model) are currently used in practical engineering calculations.

1.2 A nontraditional approach

The previous discussion has centered on temporal measurements made at a single position in space, as this has been the only measure available in RIC engines using either hot-wire or laser Doppler anemometry. However, it is now possible to measure two-dimensional velocities over an extended region at one instant in time using particle image velocimetry, PIV (Reuss, *et al.* 1989, and Reuss, *et al.* 1990). Two-dimensional spatial filtering techniques have been applied to this data to reveal velocity structures on the order of the turbulent integral-length scale that were not apparent in the instantaneous data. Further, vorticity and strain-rate distributions computed from the measured instantaneous-velocity gradients (not filtered) show a strong correspondence to the velocity structures revealed by spatial filtering. These

results stimulated the notion that spatial filtering of the velocity distribution or the use of the vorticity and strain-rate distributions might offer a means to separate the turbulence velocity fluctuations (expected to affect flame wrinkling and turbulence dissipation) from the cyclic fluctuations and ensemble-mean velocities.

The use of the filtered-velocity, vorticity, or strain-rate distributions to define turbulence tacitly assumes that the turbulence is made up of coherent structures. The concept of coherent structures in turbulence is not new (Hussain 1986). The existence and topological mapping of the coherent structures in three-dimensional direct numerical-simulations of turbulent flows has been under study for some time (Hunt, *et al.* 1988, Adrian & Moin 1988, Chong, *et al.* 1990, Chen, *et al.* 1990, and Kim & Hussain 1992). Topological mapping is an important tool to help understand the physical mechanisms that produce turbulent dissipation, mixing, and flame wrinkling. However, engineering calculations and measurements in the foreseeable future will require that the turbulence be characterized by statistical sampling of the velocity. The concept that turbulent flow is made up of coherent structures rather than totally random velocity fluctuations does not conflict with the traditional view. Sampling at one point as a function of time involves sampling of the coherent structures as they randomly pass by the sampling point. Thus, the existence of temporal and spatial correlations in turbulent measurements is consistent with the existence of coherent structures.

The ultimate goal is to explore a means for sampling the coherent structures that will provide a measure of the turbulence properties that contribute to flame wrinkling and turbulence dissipation and will also provide a rational separation of the mean flow and turbulence in RIC engines. As a first step, this study focuses on vortices or "eddy zones" as labeled by Hunt *et al.* (1988). In particular, an attempt is made to quantify the scale and intensity of the velocity associated with an "average vortex" by conditionally sampling the instantaneous velocity distribution at the position of each local maximum in the vorticity distribution. This approach is justified because the vorticity computed from the instantaneous flow reveals all vortices (rotational flow regions) found in the high-pass filtered velocity, and, even in the RIC engine flows (Reuss, *et al.* 1989, and Reuss, *et al.* 1990), the mean flow vorticity is negligible compared to the vorticity associated with the turbulent structures. Therefore, the conditional sampling is a filter-independent means to identify the position of the vortex structures. Both scale and intensity of the velocity associated with the average vortex are quantified (rather than the vorticity alone) because: one, it is the velocity that is required for closure in most engineering models, and two, the scale and the energy spectrum of the velocity is known to peak at low wave numbers while the energy spectrum of the vorticity is expected to follow that of the dissipation and therefore peak at high wave numbers (see discussions in Reuss, *et al.* 1989, and Tennekes & Lumley 1972).

It is recognized that vortex structures are by no means the only structures as indicated in the topological mappings of Hunt *et al.* (1988) and Chong et al. (1990). Further, it is recognized that the strain rate is associated with the turbulence dissipation and flame stretching. However, vortices are dominant structures in both

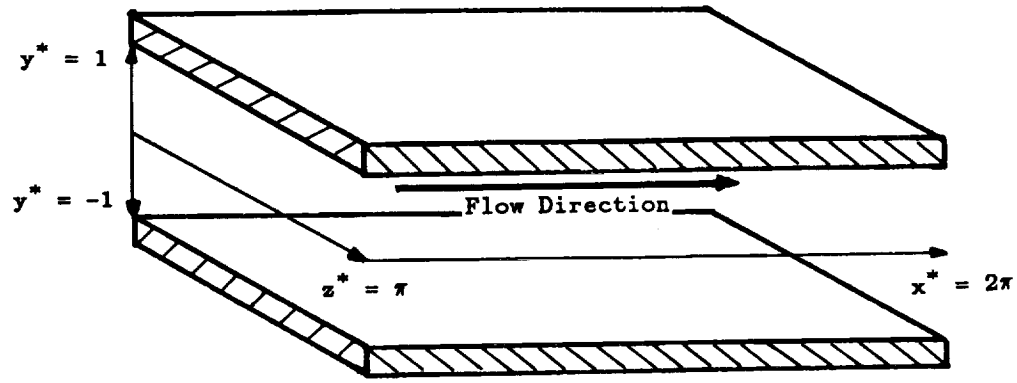

FIGURE 1. Schematic defining the channel coordinates and flow direction.

free shear and near wall flows (Chong, *et al.* 1990 and Smith, *et al.* 1991), strongly correlated with the dissipation (Chen, *et al.* 1990), and believed to be important in flame wrinkling and quenching (Poinsot, *et al.* 1990 & Rutland 1989). Both filtering and conditional sampling are used to separate the vortex velocity from the instantaneous velocity in a two-dimensional sample of a computed, three-dimensional, steady channel flow. First, the high-pass-filtered velocity distributions with different cutoff frequencies are compared to reveal the content of different spatial scales. The filtered velocity distributions are compared with the vorticity distribution to reveal the correspondence between the two. Second, the instantaneous velocity is conditionally sampled on the peaks in the vorticity distribution and ensemble averaged to yield the vorticity and velocity of the "average vortex". The strategy here is to test these two methods in a fully resolved flow where traditional measures are also valid before applying them to RIC engine data. A description of and justification for these two methods is given in Sections 3 and 4.

2. The computed channel flow

The flow geometry and coordinate direction of the computed channel flow are illustrated in Fig. 1. The channel flow is similar to that described by Kim, et.al. (1987) but with a high Reynolds number, $Re)_c = 7860$, where $Re)_c$ is based on the channel half-width, δ , and the centerline velocity $\overline{u}_c$ and $Re)_\tau = 395$ is based on δ and the wall shear velocity, $u_\tau = [\nu(du/dy)_{\text{wall}}]^{1/2}$. The computational mesh spacing is $\Delta x^+ \approx 10$ and $\Delta z^+ \approx 6^\dagger$ over the domain $0 \leq x^* < 2\pi$ and $0 \leq z^* < 2\pi$, respectively. In the y direction (normal to the wall), a nonuniform mesh is used

† Here superscript + indicates nondimensionalization by wall shear units, and superscript * by the channel thickness, eg. $x^+ = xu_\tau/\nu) = x^* Re)_\tau$ and $x^* = x/\delta$.

where $y_j^* = [(j-1)\pi/(N-1)]$, $j = 1 \ldots 193$, over the domain $-1 < y^* \leq 1$ ($y^* = 0$ at the center). The governing equations and spectral solution method are detailed in Kim, *et al.* (1987).

The velocity was sampled in the $x-z$ plane (parallel to the wall) at the center of the channel for the last computational-time step. Thus the turbulence is expected to be statistically homogeneous in both directions. All three velocity components and nine gradient tensor components are available at each mesh point. However, only the in-plane velocities, u and w, and out of plane vorticity, ω_z were used since these will be the only components available when ultimately applied to PIV measurements. Strain rates were not considered.

A summary of the statistical properties of this flow are given in Table 1. The first column gives results from statistics taken over many realizations of this flow, while the second column gives statistics computed for the particular $x-z$ plane used in this study, which is the last realization from the calculation. The integral-length scales were found from the two-point-correlation functions by choosing the x^* or z^* separation at the e^{-1} point in the correlation function. It should be noted that the longitudinal-correlation function in the z^* direction (used to determine $L_{ww})_z$) asymptotically approaches approximately 0.13 rather than zero as it should. This indicates that a residual mean (or at least a very large-scale) velocity must exist in the z^* direction, which also appeared in $\overline{w}$ for this realization. There also appears to be a discrepancy in the value of w_{rms} computed in this final realization and that averaged over many realizations.

3. Turbulence structures from spatial filtering

Spatial filtering of the two-dimensional, instantaneous-velocity distribution is a means to separate large and small scale structures, ie.

$$u(x,z) = u_l(x,z) + u_h(x,z) \tag{5}$$

where u_l and u_h are the low- and high-pass filtered velocity distributions corresponding to the large and small scale structures, respectively. This decomposition has been used for analysis of computed (Hunt, *et al.* 1988) and experimental data (Reuss, *et al.* 1989, and Reuss, *et al.* 1990). Further, Germano (1992) recently treated the filtered Navier-Stokes equations rigorously, relating the filtered velocity to the interpretation of Large Eddy Simulations results.

3.1 Computing the filtered-velocity distribution

In this study, u_l was computed from u and u_h was then determined from eqn. 5. u_l can be computed in a manner analogous to temporal signal processing by taking the two-dimensional, spatial Fourier transform of u, setting to zero all Fourier components above a desired spatial-frequency cutoff, and inverse transforming back to the real- space domain (Reuss, *et al.*, 1989). However, here the low-pass filtering was performed in the real-space domain by computing the two-dimensional local-average velocity at each mesh point as in Reuss, *et al.* (1990). This is accomplished by convolution of the instantaneous velocity distribution with an axisymmetric Gaussian kernel,

Table 1. Statistical properties of the channel flow for the centerline $x - z$ plane using many realizations or the last realization, which was studied here.

Label		Averaging Many	Plane(s) Last
Velocity	$\overline{u}^+$	20.004	19.76
	$u_{\rm rms}$	0.805	0.809
	$\overline{w}^+$	—	0.098
	$w_{\rm rms}$	0.671	0.595
Vorticity	$\overline{\omega}$	—	1.E-13
	$u_{\rm rms}$	—	10.9
Integral-	$L_{uu})_x$	0.34	—
Length	$L_{ww})_x$	0.21	—
Scale*	$L_{uu})_z$	0.18	—
	$L_{ww})_z$	0.24	—

* Determined as the 1/e point of the one-dimensional, two-point, spatial autocorrelation.

$$g(x,z) = \exp[-(x^2 + z^2)/2A^2] \tag{6}$$

where A sets the cutoff frequency of the filter by adjusting the radius, d_{cf}, at which $w(x,z) = e - 2$. The kernel was evaluated to values of x^* and z^* that were twice that of the diameter of d_{cf}. The spatial frequency content of the low-pass filtered velocity is, therefore, a Gaussian-weighted, local average. This local averaging is equivalent to a windowed Fourier transform filter using the Fourier transform pair of the Gaussian kernel (itself Gaussian)

$$G(k_x, k_z) = (2\pi A^2)^{1/2} \exp[-\pi^2 A^2 (k_x^2 + k_z^2)/4] \tag{7}$$

for the spatial-frequency cutoff, where k_x and k_z are the spatial frequencies in the x and z directions, respectively. Local averaging is considerably simpler than the Fourier transform method for flame studies (its ultimate use) where the position

of the unburned gas boundary is arbitrary, discontinuous, and multivalued in both directions (Reuss, *et al.* 1990).

The use of the spatial average also suggests a more physical interpretation of the high-pass-filtered velocity. In particular, in the limit of a very large filter, $d_{cf} \rightarrow \infty$, the low-pass velocity is the spatial-mean velocity, which should be equal to the temporal mean for the $x - z$ plane. Thus the high-pass velocity is the velocity measured by an observer moving at the mean velocity at every point in the flow. As d_{cf} is decreased the velocity of the observer varies from the mean and approaches the instantaneous value at each point. Thus, in the limit $d_{cf} \rightarrow 0$, the observer is moving at the instantaneous velocity at each point and the high-pass velocity is zero everywhere.

3.2 Filtered-velocity results

The instantaneous and high-pass-filtered velocities for $d_{cf} = 0.74$ are shown in Figs. 2a and 2c for a sub-region of the $x - z$ plane at the center of the channel. The vector scale numbers indicate the magnitude of the vector scale used in each plot relative to those in of the instantaneous velocity distribution plot (Fig. 2a); e.g, a vector in Fig. 2b has a magnitude 0.3 times that of a vector of equal length in Fig. 2a. Comparison of these two figures demonstrates the ability of the filtering to reveal structures in the flow that one would normally associate with turbulence. In particular, "eddy zones" (vortices) and "streaming zones" (directed flows between the vortices as defined by Hunt et.al 1988) are readily apparent, and the size of these structures is on the order of the integral length scales listed in Table 1. Also shown in these figures is the vorticity distribution computed from the instantaneous velocity-gradient distribution. The red and blue patches indicate regions of positive vorticity (counter-clockwise rotation) and negative vorticity (clockwise rotation), respectively. As in the previous studies (Reuss, *et al.* 1989, and Reuss, *et al.* 1990) there is a direct correspondence between the velocity vortex in the high-pass-filtered velocity distributions and the regions of high vorticity, both in sign and position.

The existence of flow structures observable in the high-pass- filtered velocity distributions for $d_{cf} > 0.74$ was not as sensitive to the filter cutoff frequency as for the RIC engine data in Reuss, *et al.* (1989). This can be seen by comparing Fig. 2b, which was derived by subtracting the mean velocity ($d_{cf} \rightarrow \infty$), from the instantaneous velocity, and Fig. 2c where $d_{cf} = 0.74$. Although there are differences in the magnitude (note the vector scales used for each plot) and direction of the velocity vectors, the same flow structures are revealed. This is expected because in the channel flow there are no mean-velocity gradients in the $x - z$ plane as in the RIC engine of Reuss, *et al.* (1989) and hence, the scales of the mean flow and turbulence in this channel flow are widely separated. However, for higher frequency-cutoff filters, $d_{cf} < 0.74$, new structures did appear while the old structures remained (albeit with altered velocity vectors). Note the two regions around $(x, z) = (3.1, 1.55)$ and $(x, z) = (3.2, 1.15)$ in Figs. 2c and 2d. For $d_{cf} = 0.74$, these two regions of the flow structures appear as streaming zones, whereas for $d_{cf} = 0.1$ smaller-scale less-intense vortices appeared. These smaller vortices cannot be disregarded as unimportant, since the peak vorticity in these two regions is -16 and

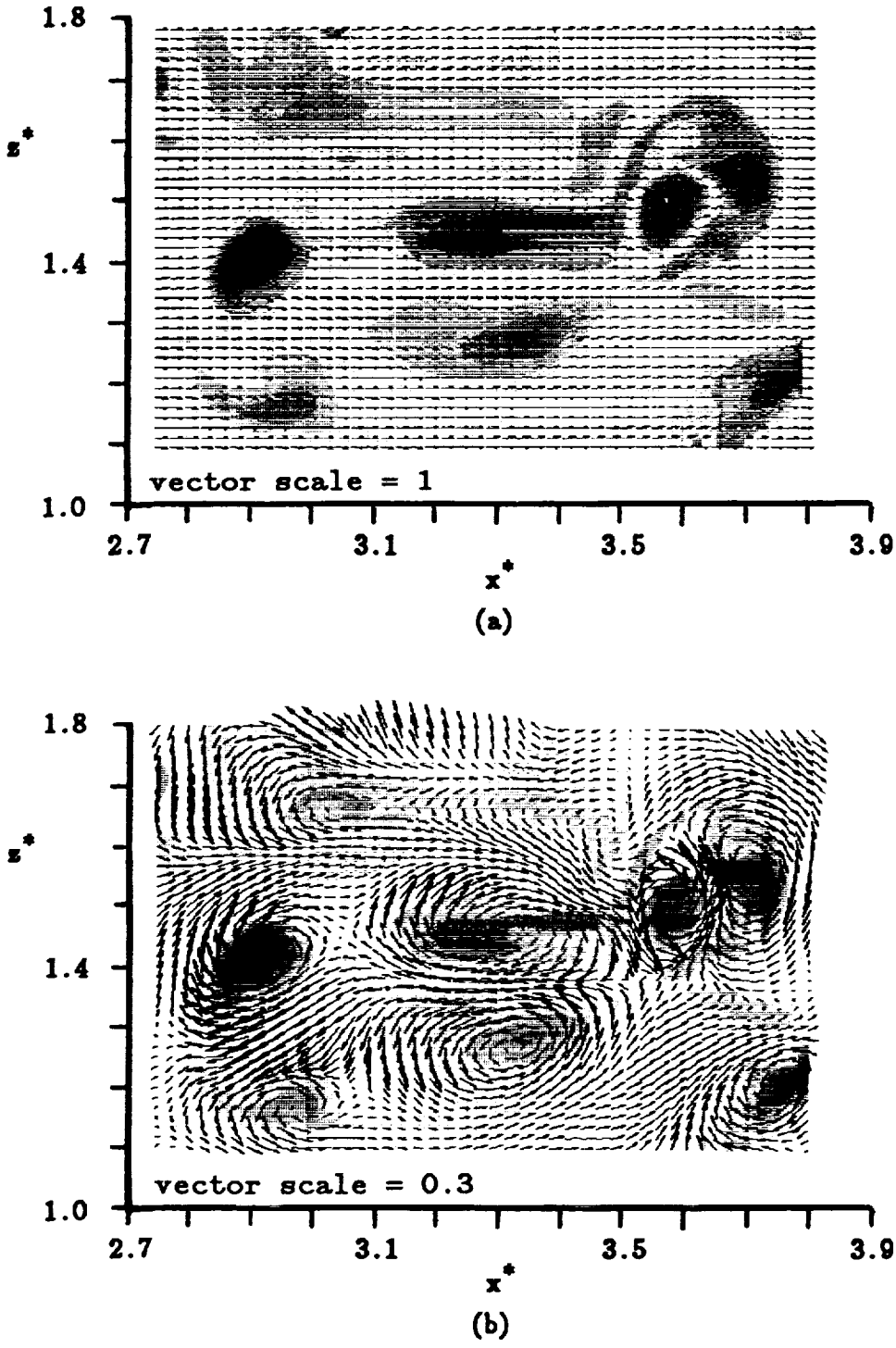

FIGURE 2 A AND B. Composite of the vorticity contours and velocity distributions for a subregion of the $x - z$ plane at $y^* = 0$. The white areas of the contours indicate regions of near zero vorticity. (a) Instantaneous velocity, (b) Mean velocity subtracted, $d_{cf} = \infty$.

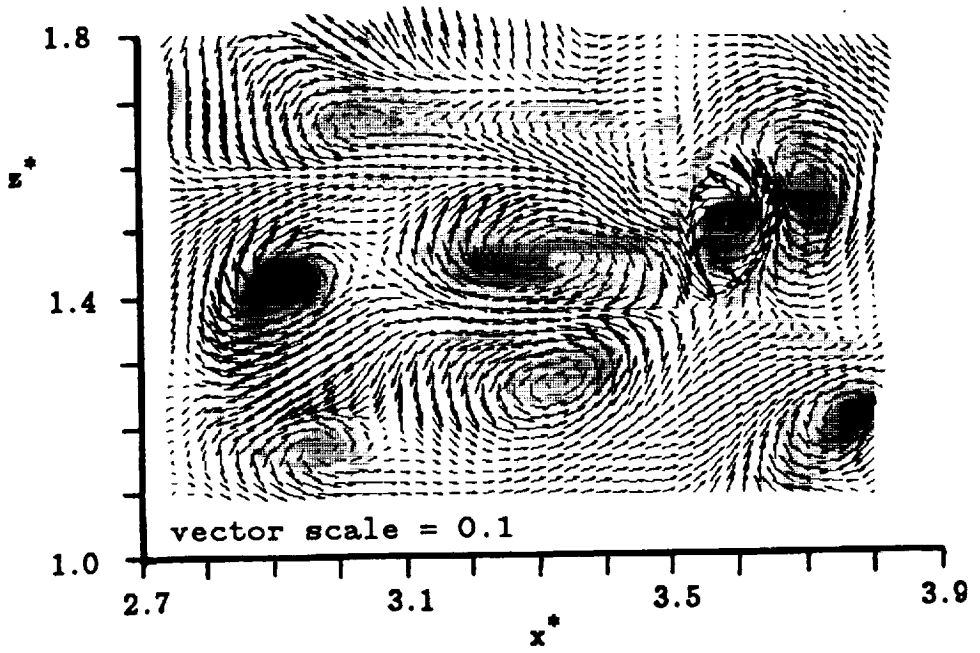

(c)

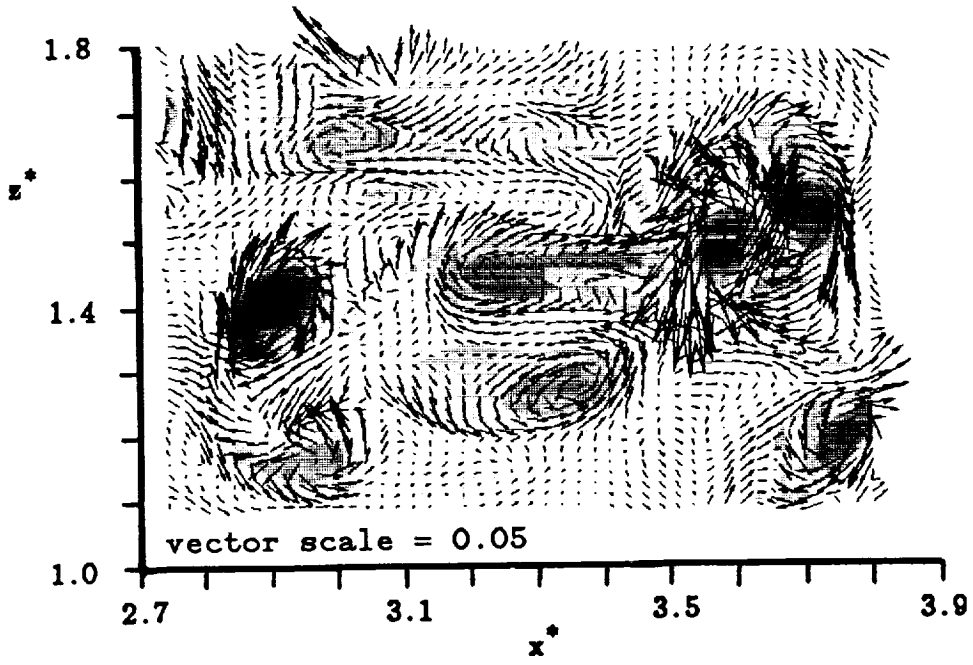

(d)

FIGURE 2 C AND D. Composite of the vorticity contours and velocity distributions for a subregion of the $x-z$ plane at $y^* = 0$. The white areas of the contours indicate regions of near zero vorticity. (c) High-pass filtered velocity with $d_{cf} = 0.74$ (d) High-pass filtered velocity with $d_{cf} = 0.1$.

+12, respectively. This is on the order of $\omega_{rms} = 10.9$ and vortices with this level of vorticity did appear with the $d_{cf} = 0.74$ filter in other regions of the $x - z$ plane. Thus, the filter cutoff can be adjusted to reveal vortices of different scales, but can miss some if applied at too low a cutoff frequency.

3.3 Discussion of the filtered-velocity results

The results of the previous section have two important implications about the usefulness of filtering. First the results demonstrated that filtering would in fact isolate vortices in the velocity distribution and on different scales, thus revealing in this channel flow the same types of flow structures observed in direct-numerical simulations of homogeneous stationary turbulence (Hunt, et al. 1988). It is tempting to contrive a method to quantify the scale and intensity of the vortices using the high-pass-filtered velocity distributions. However, even here where the mean and turbulence scales are clearly separated, both the existence of the vortex structures and the magnitude and direction of the associated vectors are dependent on the cutoff frequency. In particular, if the cutoff frequency is too low (d_{cf} large), small scale structures may be missed. If the cutoff frequency is increased (d_{cf} decreased) to assure that the smallest scale structures are revealed, the magnitude of the velocity vectors (and, therefore, any measure of the turbulence intensity) will be too low. Consequently, any quantitative measure of the scale and intensity based on the filtered velocity would be dependent on the choice of the filter cutoff frequency and does not offer a viable solution to the problems of the RIC engine. The second important finding is that the patches of vorticity, computed from the unfiltered (instantaneous) velocity distribution, identified all vortices (in the original contour plots) even though some did not appear in the filtered velocity distribution until a sufficiently high frequency cutoff was used. This suggests that the vorticity could provide a filter-independent detector of the existence of a vortex.

4. The velocity scale and intensity of the average vortex

To quantify the scale and intensity of the vortices, the instantaneous velocity distribution of the entire $x-z$ plane was conditionally sampled at the (x, z) location of the peak vorticity within each vorticity patch in the $x - z$ plane. A vorticity patch was defined as a local region with vorticity of like sign (eg. the blue and red patches in Fig. 2), and the (x, z) position selected at the peak vorticity within that patch. In some cases two peaks existed within each patch, in which case both were identified, eg. (3.05,1.55) and (3.35,1.55). Vortex detection by the vorticity peak is, in principle, a variation of the method of Hunt, *et al.* (1988) where "eddy zones" were defined by two criteria: one, the irrotational straining is small compared to the vorticity, and two, simultaneously the (local) pressure tends to a minimum somewhere in the zone. Their approach was not used here since it requires both the three-dimensional deformation tensor and the pressure distribution, which are not available from measurements. Although the simpler approach used here is less formal, it is not necessarily less rigorous or less valid for identification of vortices. The velocity distribution in Fig. 4 of Hunt, *et al.* (1988) shows regions of rotating flow structures that were not detected as eddy zones by the above criterion, as well

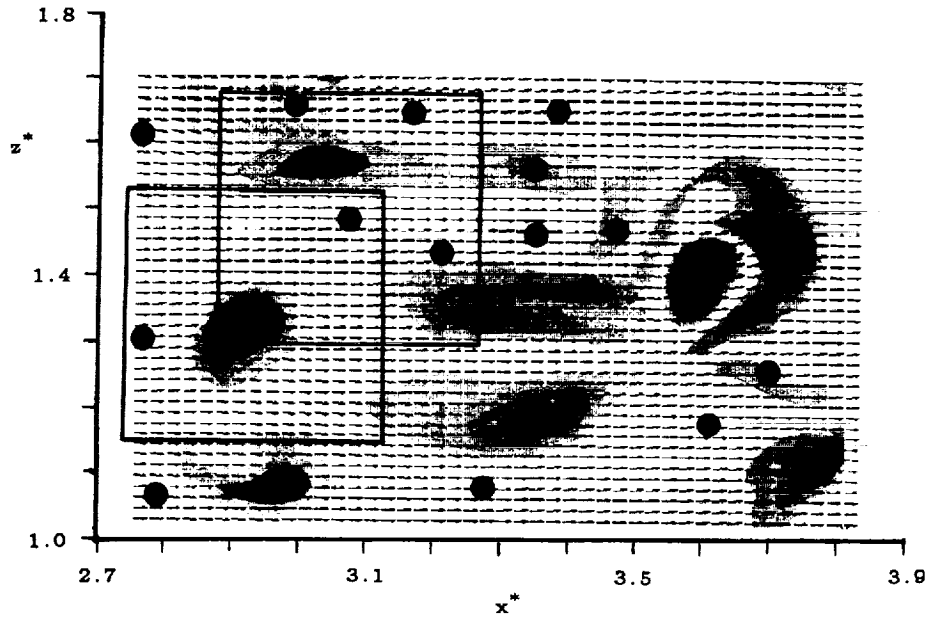

(a)

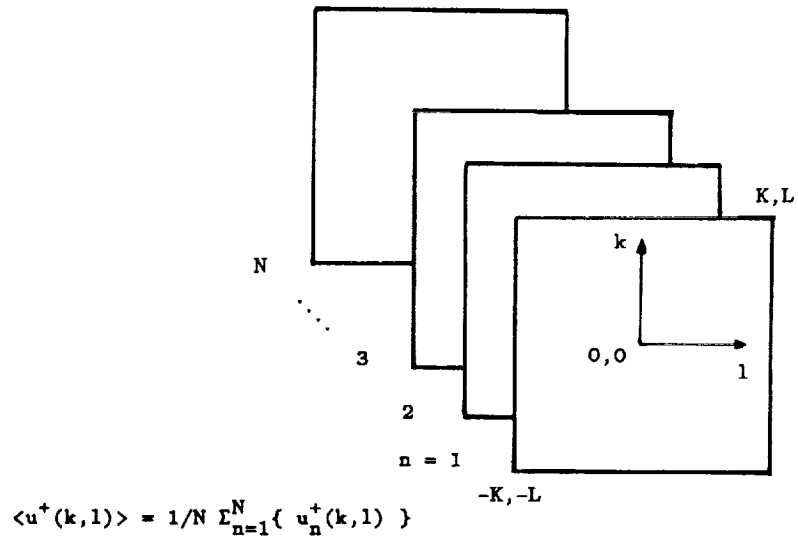

(b)

FIGURE 3. Schematic representation of (a) two conditional sampling windows (not to scale) and (b) ensemble averaging.

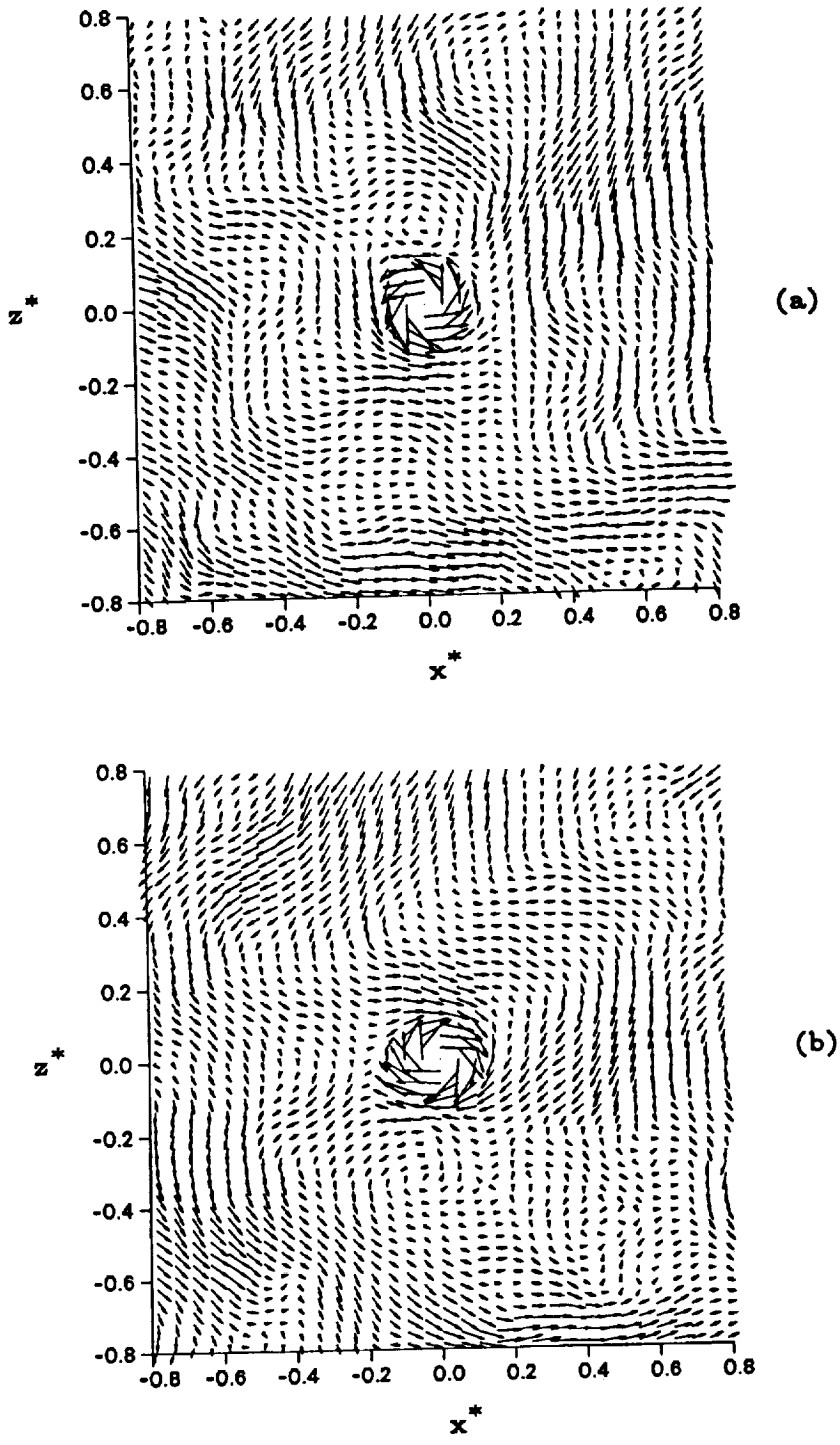

FIGURE 4. Velocity distribution of (a) the average positive vortex and (b) the average negative vortex.

as the converse. By contrast, all regions with vorticity above 10 percent of the rms value were detected regardless of the dissipation or pressure fields, and there was excellent agreement between the vorticity patches and the rotating structures in the velocity field.

The position of the peak vorticity within each vorticity patch was found manually with the aid of an interactive image processor. The dots in Fig. 3a indicate the positions of the vorticity peaks in the subregion. The instantaneous velocity distribution was conditionally sampled at these positions as follows. A square window was centered at each vorticity peak position, $\omega_p(i,j)$ and overlaid on the x,z mesh as depicted in Fig. 3a. The size of the window ($x^* = z^* = 1.6$) was chosen to be large compared to the integral length scale. The u^+,and w^+, values at each point of the window grid, (k,l), were stored. This was repeated at all $N = 597$ vorticity peak positions. The velocities at each grid location within each of the windows were then ensemble averaged by summing over all N windows (Fig. 3b) as

$$\langle u^+(k,l)\rangle = \frac{1}{N}\sum_{n=1}^{N}[(u^+(k,l)|k = 1 = 0 \;@\; \pm\omega_p(i,j)] \tag{8}$$

where the vertical bar signifies the conditional average and ω_p indicates conditioning on plus and minus vorticity. Thus two ensemble averages were computed resulting in both an average-positive and an average-negative vortex. The quantities $\langle \mathrm{w}^+(k,l)\rangle$ and $\langle\omega(k,l)\rangle$ were averaged in a like manner. Near the edges of the $x-z$ plane the window overlaps the boundary. In these regions the value of N at each k,l mesh point outside the boundary is decreased to be consistent with the number of samples at each point.

4.2 Conditional-sampling results and discussion

The velocity distribution of the positive and negative, conditionally sampled, ensemble-averaged windows are shown in Fig. 4a and b. $\langle u^+(0,0)\rangle$ has been subtracted at each point so that the observer is moving at the same velocity as the center of the average vortex. The strong positive (and negative, respectively) rotation about the center of the ensemble-average windows is immediately apparent. The velocity magnitudes, u^+ and w^+, along the x^* and z^* axes are plotted in Figs. 5a and 6a for the positive ensemble-averaged window. Only the values for the average positive vortex are presented here as the average negative vortex plots are approximately equal but opposite in sign. Again, the rotation is apparent in the lateral velocity components $u^+(0,z^*)$ and $\mathrm{w}^+(x^*,0)$. The peak lateral velocities of the average vortex were small, ≈ 0.3, compared to the statistical fluctuation value $\omega_{rms} = 0.6$. The ensemble-average vorticity along the axes is shown in Figs. 5b, and 6b as well. The peak values of the average-positive and average-negative vortices were $\langle\omega_p\rangle = \pm 18$ and the mean average vorticity,

$$\overline{\langle\omega\rangle} = \int_a^b \omega(x,0)dx^* \tag{9}$$

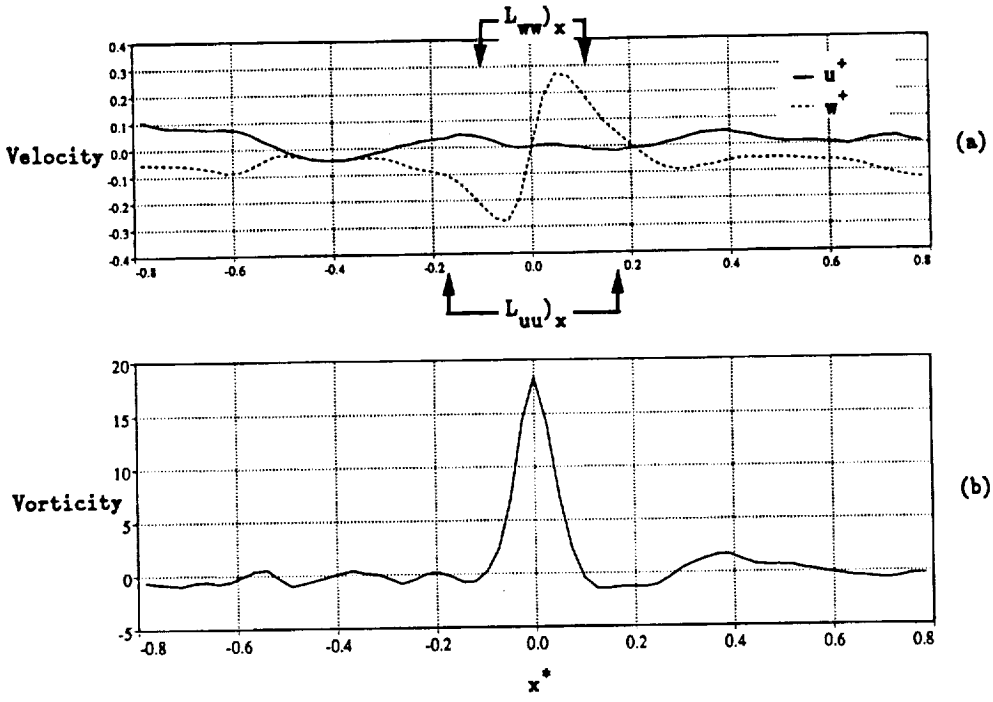

FIGURE 5. (a) The velocity, $u^+(x^*,0)$ and $w^+(x^*,0)$, and (b) vorticity, $\omega(x^*,0)$, along the x^* axis for the average positive vortex in Fig. 4a.

was approximately 7.9, where a and b were the zero crossings of the center vorticity peak. These values bracket the traditional statistical rms of the vorticity over the $x-z$ plane, $\omega_{rms} = 10.9$.

It was surprising that there was so much structured flow outside the immediate vicinity of the center vortex. In particular, on average there are streaming regions (Hunt, *et al.*) outside the center vortex with velocities as large as 1/3 the peak velocity in the vortex. In general, the streaming regions adjacent to the center vortex are directed with its rotation; however, the vorticity in the streaming regions is relatively small (cf. Figs. 5b and 6b). The existence of streaming flows outside the center vortex may be reasonable since this is observed in the composites of the vorticity and high-pass filtered distributions (cf. Fig. 2). In particular, observation of any given vortex structure reveals that it is surrounded by neighboring (adjacent) vortices, separated by a distance approximately equal to the size of the vorticity patches, with streaming flows between them. If one assumes that over many conditionally sampled vortex peaks the neighboring vortices are randomly distributed azimuthally, then the neighboring vortex structures would be expected to average

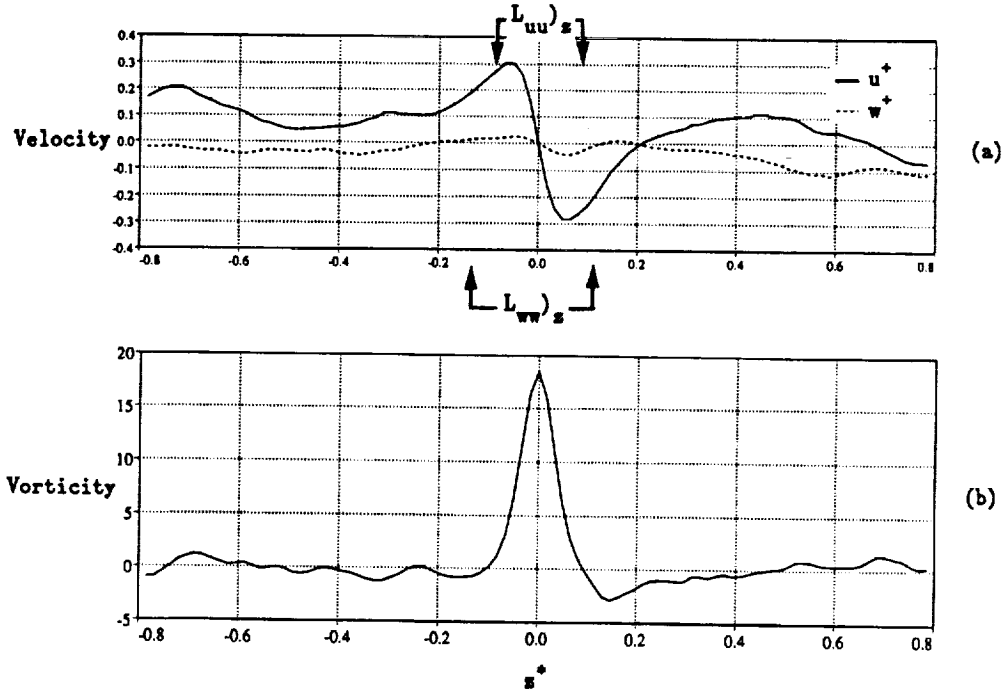

FIGURE 6. (a) The velocity, $u^+(0, z^*)$ and $w^+(0, z^*)$, and (b) vorticity, $\omega(0, z^*)$, along the z^* axis for the average positive vortex in Fig. 4a.

to zero with a large enough sample while average-steaming regions might remain. However, it is still surprising that the streaming regions exist at distances from the center vortex that are large compared to the size of the center vortex.

Most surprising was the fact that the center positive (negative) vortex is paired with an adjacent negative (positive) vortex in the positive (negative) z^* direction. The peak tangential velocity of the negative (positive) paired vortex (ie. u at $z^* \approx +0.3$ in Fig. 6a) is about 1/3 that of the peak tangential velocity of the center vortex, and the peak vorticity is about 1/7 (cf. Fig. 6b). The existence of this pair is surprising because the z^* direction should be statistically homogeneous, and it is not obvious why vortex pairs would preferentially couple with the positive vortex to the $-z^*$ side of the negative vortex. The existence of the structure and in particular the paired vortex outside the center vortex may be: one, an indication that the sample size was too small, or two, another manifestation of the flow properties in the z^* direction that resulted in the unexpected statistical properties discussed in Section 2.

The spatial scale of the vorticity associated with the average vortex is expected

to be smaller than that of the velocity as noted earlier, and this is clearly true of the average vortex since the spatial extent of the vorticity is approximately 1/2 the spatial extent of the velocity distributions in Figs. 5 and 6. To quantitatively compare the scale of the average-vortex velocity distribution with two point correlation is difficult as there is no rigorous means available. However, the lateral and longitudinal length scales in the x^* and z^* directions are indicated on the top and bottom Figs. 5a and 6a. There are no well defined structures in the longitudinal velocities, $u^+(x^*,0)$ and $\mathrm{w}^+(0,z^*)$. The spatial extent of the lateral velocity components, $u^+(0,z^*)$ and $\mathrm{w}^+(x^*,0)$, is on the order of the longitudinal and lateral-integral-length scales, $Luu)z$ and $L\mathrm{ww})x$. However, neither the differences between the lateral- and longitudinal-integral-length scales nor the anisotropy of the length scales between the x^* and z^* directions is obvious in the conditionally sampled data.

5. Conclusions

The spatial filtering and conditional sampling of the instantaneous velocity distribution were used to identify and quantify the vorticity structures in a computed channel flow. The spatial filtering revealed the vortices in the velocity distribution but required the application of different filter-cutoff frequencies to identify vortices of all scales. By contrast, conditional sampling the instantaneous, two- dimensional, velocity distribution at the vorticity-peak positions is a means to separate the vorticity structures associated with turbulence in a way that is independent of the cut-off frequency associated with filtering. The properties of the average-positive and average-negative vortices studied here are on the order of the traditional single-point time-averaged measures but do not provide an alternative for quantifying those values.

The average-positive and average-negative vorticity distributions are equal and opposite in value and are, therefore, consistent with the traditional- statistical-mean value of zero. However, the peak-average-vorticity, $\langle\omega_p\rangle = \pm 18$, and mean average vorticity, $\overline{\langle\omega\rangle} = 7.9$, differ from but bracket the traditional statistical value, $\omega_{\mathrm{rms}} = 10.9$. A rigorous derivation of the correspondence between the traditional and conditionally-sampled values might resolve this difference. The peak velocity associated with the average vorticity was half the traditional rms velocity fluctuation. The spatial extent of the velocity distributions were on the order of the traditional lateral-length scales and somewhat smaller than the streamwise longitudinal length scales. This suggests that the vorticity structures are within the size of the structures sampled in two-point correlations but are themselves insufficient to explain either the full extent of the scale or the anisotropy measured by the two-point correlations. Larger structures must coexist and/or structures outside but adjacent to the average vortex must contribute to the two point correlations.

Acknowledgements

Support was provided by The Center for Turbulence Research and General Motors Research and Environmental Staff. We would like to thank Prof. Hugh Blackburn,

Dr. Todd D. Fansler, Dr. John Kim, and Minami Yoda for their help and consultation. A special thank you is extended to Prof. Brian D. Cantwell for his guidance during the summer program.

REFERENCES

ADRIAN, R. J. & MOIN, P. 1988 Stochastic Estimation of Organized Turbulent Structure: Homogeneous Shear Flow,. *J. Fluid. Mech.* **190,** 531.

ARCOUMANIS AND WHITELAW, J. H., 1987 Fluid Mechanics of Internal Combustion Engines – A Review. *Proc. I. Mech. E.* **201C,** 57.

CHEN, J. H., CHONG, M. S., SORIA, J., SONDERGAARD, R., PERRY, A. E., ROGERS, M., MOSER, R., & CANTWELL, B. J. 1990 A Study of the Topology of Dissipating Motions in Direct Numerical Simulations of Time-Developing Compressible and Incompressible Mixing Layers. In*Report CTR-S90, Proceedings of the 1990 Summer Program, Center for Turbulence Research, Stanford University & NASA Ames.*

CHONG, M. S., PERRY, A. E., & CANTWELL, B. J. 1990 A General Classification of Three-Dimensional Flow Fields. *Phys. Fluids A* . **2(5).**

FANSLER, T. D., AND FRENCH, D. T. 1988 Cycle-Resolved Laser-Velocimetry Measurements in a Reentrant-Bowl-in-Piston Engine. *SAE Paper 880377.*

FANSLER, T.D. 1993 Turbulence Production and Relaxation in Bowl-In- Piston Engines. Submitted to 1993 SAE International Congress.

FRASER, R. A., AND BRACCO, F. V. 1988 Cycle-Resolved LDV Integral Length-Scale Measurements in an I. C. Engine. *SAE Paper 880021.*

GERMANO, M. 1992 Turbulence: The Filtering Approach. *J. Fluid. Mech.* **238,** 325.

GLOVER, A. R. 1986 Towards Bias-Free Estimates of Turbulence in Engines. *Third International Symposium on Applications of Laser Anemometry to Fluid Mechanics.* Lisbon, Portugal.

HUNT, J. C. R., WRAY, A. A., & MOIN, P. 1988 Eddies, Streams, and Convergence Zones in Turbulent Flows. In*it Report CTR-S88, Proceedings of the 1988 Summer Program, Center for Turbulence Research, Stanford University & NASA Ames.*

HUSSAIN, A. K. M. F. 1986 Coherent Structures and Turbulence. *J. Fluid. Mech.* **173,** 303.

KIM, J., AND HUSSAIN, A. K. M. F. 1992 Propagation Velocity and Space-Time Correlation of Perturbations in Turbulent Channel Flow. *NASA Tech. Mem.* TM 103932.

KIM, J., MOIN, P., & MOSER, R. 1987 Turbulence Statistics in Fully Developed Channel Flow at Low Reynolds Number. *J. Fluid Mech.* **177,** 133.

LE COZ, J. F. 1992 Cycle-to-Cycle Correlations Between Flow Field and Combustion Initiation in an S. I. Engine. *SAE Paper 920517.*

POINSOT, T., VEYNANTE, D., & CANDEL, S. 1990 Diagrams of Premixed Turbulent Combustion Based on Direct Simulation. *23rd Symposium(International) on Combustion.* The Combustion Institute, Pittsburgh, 613.

RASK, R. B. 1981 Comparison of Window, Smoothed-Ensemble, and Cycle- by-Cycle Data Reduction Techniques for Laser Doppler Anemometry Measurements of In-Cylinder Velocity. In*Fluid Mechanics of Combustion Systems,* T. Morel, R. P. Lohmann & J. M. Rackley, ed., ASME, NY.

RASK, R. B. 1984 Laser Doppler Anemometry Measurements of Mean Velocity and Turbulence in Internal Combustion Engines. In*Intl. Conf. on Applic. of Lasers and Electro-Optics,* Boston, Nov. 12-15, Also available at GM Research and Environmental Staff, Publication GMR-4839, October 3, 1984.

REUSS, D. L., ADRIAN, R. J., LANDRETH, C. C., FRENCH, D. T., & FANSLER, T. D. 1989 Instantaneous Planar Measurements of Velocity and Large-Scale Vorticity and Strain Rate in an Engine Using Particle Image Velocimetry. *SAE Paper 890616.*

REUSS, D. L., BARDSLEY, M., FELTON, P. G., LANDRETH, C. C., & ADRIAN, R. J. 1990 Velocity, Vorticity and Strain-Rate Ahead of a Flame Measured in an Engine Using Particle Image Velocimetry. *SAE Paper 900053.*

RUTLAND, C. J., FERZIGER, J. H., & CANTWELL, B. J. 1989 Effects of Strain, Vorticity, and Turbulence on Premixed Flames. Ph. D Thesis, Stanford University.

SMITH, C. R., WALKER, J. D. A., HAIDARI, A. H., & SOBRUN, U. 1991 On the dynamics of Near-Wall Turbulence. *Phil. Trans. R. Soc. Lond. A.* **336,** 131.

TENNEKES, H., AND LUMLEY, J. L. 1972 *A first Course in Turbulence* MIT Press, Cambridge, Massachusetts, Chapt. 8.3, 262.